

Benchmarking Artificial Intelligence Models for Daily Coastal Hypoxia Forecasting

Magesh Rajasekaran^{1,2}, Md Saiful Sajol³, Chris Alvin⁴, Supratik Mukhopadhyay^{1,2}, Yanda Ou^{2,5}, Z. George Xue^{2,5}

¹Department of Environmental Sciences, Louisiana State University, Baton Rouge, LA, USA

²Center for Computation and Technology, Louisiana State University, Baton Rouge, LA, USA

³Department of Computer Science, Louisiana State University, Baton Rouge, LA, USA

⁴Department of Computer Science, Furman University, Greenville, SC, USA

⁵Department of Oceanography and Coastal Sciences, Louisiana State University Baton Rouge, LA, USA

February 6, 2026

Abstract

Coastal hypoxia, especially in the northern part of Gulf of Mexico, presents a persistent ecological and economic concern. Seasonal models offer coarse forecasts that miss the fine-scale variability needed for daily, responsive ecosystem management. We present study that compares four deep learning architectures for daily hypoxia classification: Bidirectional Long Short-Term Memory (BiLSTM), Medformer (Medical Transformer), Spatio-Temporal Transformer (ST-Transformer), and Temporal Convolutional Network (TCN). We trained our models with twelve years of daily hindcast data from 2009-2020. Our training data consists of 2009-2020 hindcast data from a coupled hydrodynamic-biogeochemical model. Similarly, we use hindcast data from 2020 through 2024 as a test data. We constructed classification models incorporating water column stratification, sediment oxygen consumption, and temperature-dependent decomposition rates. We evaluated each architectures using the same data preprocessing, input/output formulation, and validation protocols. Each model achieved high classification accuracy and strong discriminative ability with ST-Transformer achieving the highest performance across all metrics and tests periods (AUC-ROC: 0.982-0.992). We also employed McNemar's method to identify statistically significant dif-

ferences in model predictions. Our contribution is a reproducible framework for operational real-time hypoxia prediction that can support broader efforts in the environmental and ocean modeling systems community and in ecosystem resilience. The source code is available¹.

Deep learning, Time-series analysis, Environmental monitoring, Neural networks, Hypoxia forecasting, Louisiana-Texas shelf

1 Introduction

Dissolved oxygen concentrations below 2.0 mg/L is referred to as *coastal hypoxia* and it creates serious problems for marine ecosystems worldwide. In particular, the northern region of the Gulf of Mexico suffers from recurring seasonal hypoxic events that create “dead zones” that devastate marine life, disrupt fisheries, and impose real economic costs on coastal communities NOAA [2024]. The Louisiana-Texas shelf (Figure 1) has some of the most severe and persistent hypoxic conditions globally, driven by interactions between nutrient loading from the Mississippi River, water column stratification, and processes involving sediment oxygen demand Ou et al. [2022].

¹<https://github.com/rmagesh148/hypoxia-ai/>

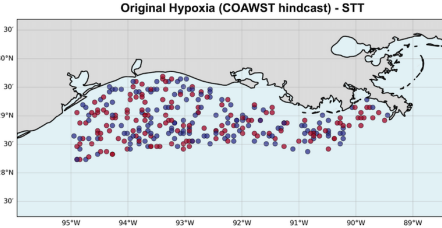


Figure 1: The spatial domain of the hindcast model used in this study: the Louisiana-Texas shelf. This image shows the random samples of COAWST hindcast hypoxia (Blue) and normoxia (Red) for the month of August 2020.

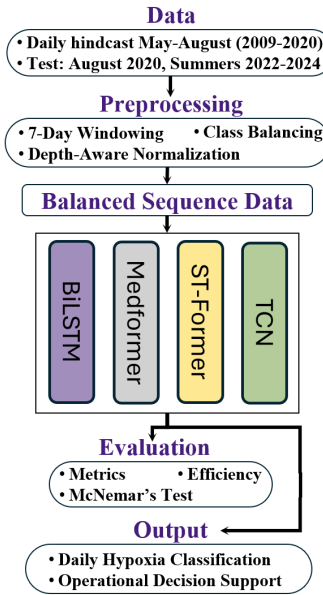


Figure 2: Conceptual workflow for daily coastal hypoxia forecasting.

Current systems for operational forecasting in the Gulf use seasonal statistical models. Temporally, monthly, or seasonal predictions are too coarse to provide useful forecasts. These approaches miss the fine-scale temporal variability that is critical for responsive ecosystem management. Since these processes operate on timescales much shorter than seasonal cy-

cles, greater temporal resolution in predictions is essential.

Daily resolution is required for operational forecasting; deep learning models can exploit temporal patterns in oceanographic time-series data to achieve this level of granularity. Sequence modeling architectures such as recurrent neural networks Graves and Schmidhuber [2005], convolutional networks Lea et al. [2016], and transformer-based models You et al. [2022], have shown success in capturing complex temporal dependencies in different domains.

This paper addresses the need for daily hypoxia forecasting by comparing four deep learning architectures within a unified experimental framework (see Figure 2). We formulate hypoxia prediction as a sequence-to-one classification task. Our models are trained to learn how environmental conditions lead to oxygen depletion. To this end, we use twelve years of daily hindcast data from a coupled hydrodynamic-biogeochemical model Warner et al. [2010]. We preprocess the daily hindcast data by (1) encoding temporal cycles, (2) normalizing, (3) creating sequences, and (4) addressing class imbalance between rare hypoxic events and the more common normoxic events. The architectures we evaluate span the spectrum of modern sequence modeling approaches: BiLSTM for capturing bidirectional temporal dependencies, TCN for efficient parallel processing of temporal sequences, Medformer for multi-scale temporal pattern recognition, and ST-Transformer for joint spatial-temporal modeling. We evaluate each model using the same framework to ensure statistical rigor in our comparisons: preprocessing, input/output formulation, and validation protocols.

Our contributions are as follows. We benchmark temporal deep learning architectures for Gulf hypoxia prediction under identical experimental conditions, allowing direct performance comparison. Second, we apply McNemar's statistical significance test to quantify differences in model predictions; this is notable as environmental AI studies often do not perform such an analysis. Third, we evaluate transformer variants (Medformer and spatio-temporal attention models) that have yet to be tested for coastal hypoxia prediction.

2 Task Overview

Our goal is to develop models that support daily operational forecasting of hypoxic conditions. We therefore formulate coastal hypoxia prediction as a binary classification problem to distinguish between hypoxic (dissolved oxygen ≤ 2.0 mg/L) and normoxic conditions in bottom waters of the Louisiana-Texas shelf. We do so using a sequence-to-one prediction framework that captures temporal dependencies in oceanographic processes. Our input features include environmental time series that influence oxygen depletion in coastal marine ecosystems.

Daily hypoxia forecasts can provide early warnings of hypoxic events for fishery managers and researchers in the field. We focus on metrics suitable for operational use: F1-score for handling class imbalance, AUC-ROC for ranking ability, and optimized accuracy thresholds to support decision-making. Our goal is to maximize detection of hypoxic events while mitigating false alarm rates.

3 Dataset and Data Preparation

3.1 The Data

We use a hindcast dataset from the Louisiana-Texas shelf covering May through August of each year from 2009 to 2020 Ou [2024], Ou et al. [2025] with further hindcast data covering 2022 through 2024. The spatiotemporal records originate from Coupled Ocean-Atmosphere-Wave-Sediment Transport (COAWST) Warner et al. [2010], a modeling pipeline tailored for the Gulf of Mexico. COAWST integrates the Regional Ocean Modeling System (ROMS) Shchepetkin and McWilliams [2005] with a revised version of the North Pacific Ecosystem Model for Understanding Regional Oceanography (NEMURO) Kishi et al. [2007].

In total, our 2009-2020 dataset contains 1471 summer records having 25km^2 spatial resolution organized as 2-dimensional matrices. We include three key input variables known to drive coastal hypoxia. Potential energy anomaly (PEA) measures water col-

umn stratification Ou et al. [2022]; higher values indicate stronger stratification that reduces oxygen supply to bottom waters. The rate of sediment oxygen consumption (SOC) Fennel et al. [2013] and the temperature-dependent decomposition rate of organic matter (DCP_{Temp}) Kätterer et al. [1998] represent two more input variables. Both variables contribute to oxygen consumption in sediments since they influence the decomposition of organic matter within sediment layers. Each of these variables are provided as multivariate time series spanning 7-day windows to capture temporal dependencies inherent in oceanographic processes.

Our models classify conditions as hypoxic (bottom-dissolved oxygen concentration is $< 2.0\text{mg/L}$) or normoxic.

3.2 Data Preparation Pipeline

Our data preparation pipeline (Figure 3) converts raw hindcast data into sequences suitable for training and testing.

Data input. We accept the hindcast matrices and organize them for sequential processing. This involves extracting the temporal coordinates from each record to enable subsequent chronological ordering and feature engineering operations.

Preprocessing and feature engineering. We transform the continuous oxygen measurements into binary classification targets and augment the temporal information through cyclical encoding. That is, for each time-scale (day of year, month, hour), we extract and convert using sine and cosine transformations to preserve seasonal and diurnal periodicity. This encoding ensures that temporal boundaries (e.g., December to January transitions, or 23:59 to 00:00 hour changes) are represented as continuous rather than discrete jumps, allowing a model to properly capture the circular nature of time. Last, all matrices undergo minimum-maximum normalization, and any spatial regions corresponding to land are masked using zeroes.

Building the Sequence Dataset. We then partition the time series data by depth to account for distinct oceanographic characteristics at each level. We split the data temporally selecting August 2020

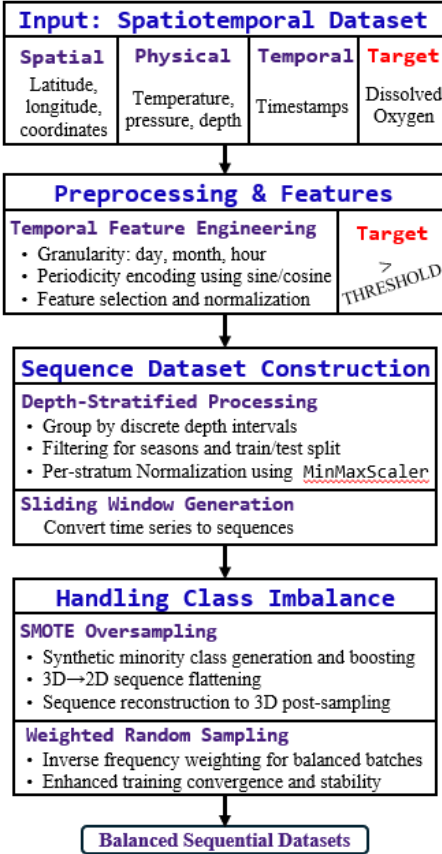


Figure 3: The data preparation workflow for our Deep Learning pipeline for time series for classification of dissolved oxygen in the Louisiana-Texas shelf.

and data from 2022-2024 as test sets; all other months from 2009 to 2020 constitute the training set. This ensures model evaluation preserves temporal integrity by relying only on ‘future’ data.

To prepare the data for sequence modeling, we segment the time series into overlapping sequences using a sliding window approach. This creates three-dimensional tensors with dimensions for samples, time steps, and features. We then normalize each depth interval independently to preserve depth-specific oceanographic patterns.

Mitigating imbalance of hypoxic events. Hypoxic events are relatively rare. To mitigate the class

imbalance in the dataset, we apply SMOTE oversampling Chawla et al. [2002], which has been successfully applied to time-series classification tasks. SMOTE requires 2D input, so we flatten each sequence by concatenating time steps and features into a single vector before generating synthetic samples. SMOTE generates synthetic minority class samples by linearly interpolating between existing samples and their nearest neighbors:

$$x_{\text{new}} = x + \mu \cdot (x_{nn} - x), \quad \mu \sim U(0, 1) \quad (1)$$

with x being a sample from a minority class, x_{nn} being one of the k nearest neighbors of x belonging to the same minority class, and μ being a random number uniformly drawn from $[0, 1]$. After oversampling, the sequences are reshaped to their original 3D temporal structure. We combine SMOTE with weighted random sampling during training (Section 5.2). SMOTE addresses imbalance at the dataset level by increasing minority class representation while weighted random sampling addresses imbalance at the batch level by ensuring balanced batch composition. The resulting training data ensures that rare hypoxic cases are adequately represented.

4 Architectures

As described in Section 3, our dataset consists of multivariate environmental observations sampled daily from 2009-2020 and in summers of 2022-2024. Hypoxia onset, persistence, and dissipation are governed by bottom-water oxygen levels NOAA [2024], Yu et al. [2015], Matli and Obenour [2024]. These factors are modulated by wind events, stratification, and river-plume dynamics that operate on shorter timescales than seasonal or interannual cycles alone. Sequence models are well-suited for these data because they capture temporal patterns and interactions among variables. In this work, we consider four architectures for daily hypoxia classification: *Bidirectional LSTM (BiLSTM)* Schuster and Paliwal [1997], Graves and Schmidhuber [2005], *Temporal Convolutional Network (TCN)* Lea et al. [2016], *Medformer*

Wang et al. [2024], and *Spatio-Temporal Transformer (ST-Transformer)* You et al. [2022].

Bidirectional LSTM. BiLSTM augments the standard LSTM with two parallel layers: one forward, one backward. This bidirectional structure captures dependencies from both past and future within the observation window, which is useful when outcomes depend on cumulative conditions rather than isolated states. The forward layer processes a sequence from past to present, with the backward layer processing from future to past. The final representation combines both temporal perspectives:

$$\vec{s}_t = \text{LSTM}_f(u_t, \vec{s}_{t-1}) \text{ Graves and Schmidhuber [2005]} \quad (2)$$

$$\overleftarrow{s}_t = \text{LSTM}_b(u_t, \overleftarrow{s}_{t+1}) \text{ Graves and Schmidhuber [2005]} \quad (3)$$

$$s_t = [\vec{s}_t; \overleftarrow{s}_t] \quad (4)$$

where \vec{s}_t and \overleftarrow{s}_t are the hidden states from the respective forward and backward passes, and s_t is their concatenation and u_t is the t th input in the sequence. The implementation uses two hidden layers, each containing 120 memory units. Dropout regularization of 30% is applied between layers to account for overfitting, while the final classification layer maps the temporal representations to binary hypoxia predictions.

Temporal Convolutional Network Recurrent architectures have long been the default for time-series modeling, yet they introduce challenges such as vanishing gradients and slow, sequential computation. TCN replaces recurrence with dilated causal convolutions, preserving temporal order while enabling parallel computation. By stacking convolutional layers with progressively increasing dilation rates across three layers, TCNs can capture long-range temporal dependencies through large receptive fields without requiring deep or computationally intensive architectures. Temporal integrity is maintained since the causal structure depends only on past and current signals. Each layer in the network applies dilated convolutions with exponentially increasing dilation rates:

$$h_t^{(l)} = \sigma \left(\sum_{k=0}^{K-1} W_k^{(l)} h_{t-d \cdot k}^{(l-1)} + b^{(l)} \right) \quad (5)$$

with K being the kernel size, d being the dilation factor, σ being nonlinear, and $h_t^{(l)}$ being the hidden activation at layer l and time t . The final classification is performed on the last temporal output, representing the most recent processed information.

Medformer. Standard models struggle to capture the multi-scale temporal patterns and variable interactions typical of environmental time series data. To address this challenge, we include Medformer, a Transformer variant designed for multivariate time series. Medformer decomposes input into temporal ‘patches’ at multiple resolutions to detect patterns across distinct time scales. Medformer also learns how different variables influence each other by embedding them together, allowing the model to understand complex relationships across multiple signals. Self-attention mechanisms with 4 heads and 2 layers allow the model to attend to the most relevant temporal segments. The attention mechanism uses masking to prevent the model from seeing future time steps:

$$Z^l = \text{softmax} \left(\frac{QK^\top}{\sqrt{d_k}} + M \right) V \quad (6)$$

where M is a masked attention bias, integrated into the standard transformer attention. To combine these insights, Medformer applies a two-stage attention mechanism: local attention identifies salient features within each scale while global attention weights contributions of each time scale to the overall representation. The result is a unified representation that can effectively handle diverse and multi-scale input data.

Spatio-temporal Transformer. ST-Transformer extends the Transformer framework by treating each variable as a spatial unit and applying attention jointly across space and time. Local attention captures interactions among spatial units (e.g., grid cells, stations), while temporal attention tracks dependencies across time. The input projection layer transforms the original features to

higher dimensional vectors suitable for attention mechanisms. The ST-Transformer first embeds input features, then applies multi-head attention with spatio-temporal encoding:

$$Z^0 = XW_e \quad (7)$$

$$Q, K, V = Z^{l-1}W_Q, Z^{l-1}W_K, Z^{l-1}W_V \quad (8)$$

$$Z^l = \text{softmax} \left(\frac{QK^\top}{\sqrt{d_k}} + A_{\text{spatial}} + A_{\text{temporal}} \right) V \quad (9)$$

where l is the number of layers, X is input data, W_e is the weight matrix, A_{spatial} encodes positional dependencies, and A_{temporal} encodes temporal dependencies.

The transformer uses 16 attention heads and 3 encoder layers, allowing the model to capture complex temporal relationships across different time scales. The final classification is performed on the mean-pooled temporal representations, effectively aggregating information across the entire sequence. This is in contrast to Medformer, which embeds variables jointly to learn cross-signal relationships without assuming spatial organization. Thus, ST-Transformer is well-suited for hypoxia prediction because it captures both spatial patterns and temporal evolution. Here, spatial dimensions represent grid cells and temporal dimensions represent observation sequences.

5 Methodology

5.1 Experimental Design and Validation Framework

We designed a validation framework using multiple models to assess the robustness of deep learning models to predict hypoxic conditions in the Gulf of Mexico (Figure 1). We partitioned the training and testing data across different time periods, enabling the model to represent temporal characteristics in the data. Since oxygen dynamics vary by depth, we processed each depth layer independently. We adopted a multi-model approach by choosing four different

neural network architectures that can handle temporal time-series data to help predict hypoxia. The temporal data are restructured using a sliding window approach that creates sequences of fixed length. Each prediction target is associated with a preceding sequence of environmental conditions. We selected a 7-day window size to align with hypoxia events, which typically develop over weekly timescales. Our training dataset covers the same months as the test ensuring seasonal pattern learning. The test data are temporarily separated from the training data to provide temporal independence.

We evaluate classification performance using Receiver Operating Characteristic Area Under the Curve (AUC-ROC), which measures how capable a model is in distinguishing between normoxic and hypoxic conditions. Our dataset is highly imbalanced with most instances being non-hypoxic data compared to hypoxic events. Therefore, we use the Precision Recall Area Under the Curve (AUC-PR), which is particularly well-suited for evaluating model performance on imbalanced datasets. Finally, we use log loss and the Brier score to understand the quality of predicted probability distribution, crucial for informed decision-making.

Our framework also includes automatic threshold optimization based on maximization of the F1-score. That is, we compute precision-recall curves across all possible thresholds and identify the optimal decision boundary that balances precision and recall. This optimization is performed independently for each model, ensuring that each architecture operates at its optimal decision threshold. We show the confusion matrices for the optimized thresholds, providing insight into the overall classification performance. The implementation computes true positives, false positives, true negatives, and false negatives, enabling detailed error analysis. This analysis is particularly important for prediction of hypoxic events, where false negatives (missed hypoxia events) and false positives (false alarms) could lead to misinformed decisions or other serious consequences.

5.2 Implementation Details

The custom data loader implementation incorporates weighted random sampling to maintain class balance during training. This complements SMOTE oversampling (Section 3.2), which addresses dataset-level imbalance while weighted sampling ensures batch-level balance. The sample weights are computed on the basis of the class frequencies, ensuring that each batch contains representative samples from both classes. To achieve class balance while maintaining the temporal integrity of the data sequences, we use PyTorch’s `WeightedRandomSampler`. ST-Transformer encodes spatial relationships between grid cells using spatial ($A_{spatial}$), and temporal relationships along 7-day sequences using ($A_{temporal}$), allowing simulational learning of where hypoxia occurs and how it evolves over time.

To ensure stable convergence when learning complex temporal patterns in oceanographic data, the training implementation uses the Adam optimizer, the learning rate being set to 0.001. The learning rate is kept constant throughout the training to maintain consistent gradient updates, which is useful for modeling temporal relationships in the data. We do not use batch normalization since it can disrupt temporal dependencies in sequential data.

The training implementation processes data in batches of 1024 sequences, balancing computational efficiency with memory constraints. Each epoch processes the entire training dataset, with loss computation performed on each batch. The implementation includes comprehensive log of training progress, including per-epoch loss values and convergence monitoring. *Early Stopping* is not implemented, as the temporal nature of the data requires full training to capture all seasonal patterns over multiple annual cycles. Our temporally separated test sets (August 2020, Summers 2022-2024) rigorously evaluate generalization without validation-based stopping. We want to ensure that the learned models can be used to simulate real-world deployments where models can predict future conditions. We successfully validated real-world deployment by testing the model with real-world data from 2022-2024.

Table 1: Hypoxia classification results for 4 time-frames.

Dataset	Model	AUC-ROC	AUC-PR	Accuracy	F1
August 2020	BiLSTM	0.986	0.825	0.974	0.744
	Medformer	0.976	0.806	0.972	0.738
	ST-Transformer	0.992	0.881	0.948	0.802
	TCN	0.974	0.784	0.970	0.712
Summer 2022	BiLSTM	0.972	0.746	0.925	0.716
	Medformer	0.955	0.755	0.656	0.702
	ST-Transformer	0.983	0.831	0.943	0.774
	TCN	0.947	0.694	0.812	0.658
Summer 2023	BiLSTM	0.981	0.736	0.935	0.704
	Medformer	0.944	0.702	0.564	0.670
	ST-Transformer	0.988	0.820	0.957	0.781
	TCN	0.956	0.720	0.614	0.701
Summer 2024	BiLSTM	0.976	0.730	0.949	0.709
	Medformer	0.962	0.718	0.877	0.661
	ST-Transformer	0.982	0.782	0.959	0.741
	TCN	0.967	0.674	0.936	0.680

6 Experimental Results and Discussion

We trained the models for different numbers of epochs, although epoch 30 was the best for each model. We then tested the trained model with the test set for August 2020 as well as summer data for 2022 to 2024.

6.1 Classification Performance Analysis

We evaluated model performance on the basis of a number of metrics. We develop and test a binary classification model that predicts hypoxia or non-hypoxia. The core performance metrics of a model is calculating the accuracy of the model itself, i.e. given the unseen data how well the model is able to predict true values. Model accuracy represents the fraction of correct predictions, although this metric can be misleading with imbalanced datasets. Table 1 shows model accuracy for each dataset. BiLSTM achieved the highest accuracy (97.4%) for August 2020 test data, but accuracy alone can be misleading for imbalanced datasets.

AUC-ROC. Since hypoxic events are rare, high accuracy may reflect correct prediction of abundant normoxic conditions rather than effectively detecting hypoxic ones. An ROC curve shows the variation of

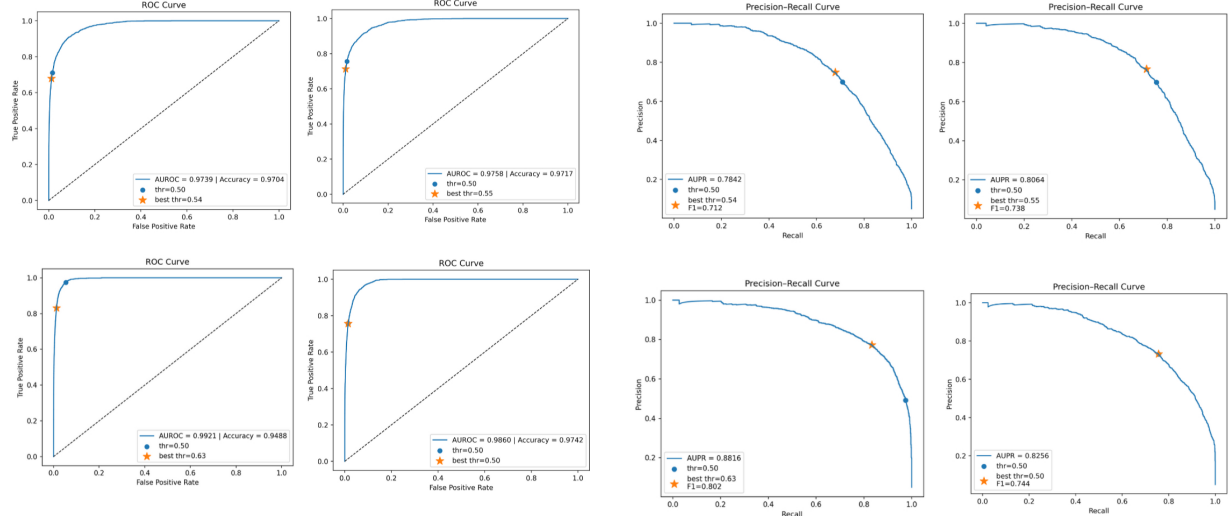


Figure 4: ROC Curve of all 4 models. *TCN* (Top Left), *Medformer* (Top Right), *STT* (Bottom Left), *BiLSTM* (Bottom Right)

the True Positive Rate with respect to the False Positive Rate for different values of the threshold, and the AUC represents the area under this curve, measures how effectively the model prioritizes positive instances over negative ones.

Figure 4 shows different ROC curve thresholds for each model using August 2020 data. We observe in Figure 4 that all models show strong discriminative ability with AUROC values ranging from 0.9739 to 0.9921 while BiLSTM is the most balanced with high AUROC (0.9860) and accuracy (0.9742).

Precision-recall and F1. AUC-ROC can be overly optimistic with class imbalance, so we also use precision-recall for model evaluation. Precision reflects the fraction of all predicted positives that were correctly identified, while recall indicates how effectively all true positives are detected. The F1 score is the harmonic mean of precision and recall, providing a single measure that balances how many predicted positives are correct with how many actual positives are recovered. Lower precision (recall) values suggest a stronger propensity to overpredict (underpredict) hypoxic conditions.

Confusion matrices. Figure 5 shows the

Figure 5: PR Curve of all 4 models. *TCN* (Top Left), *Medformer* (Top Right), *STT* (Bottom Left), *BiLSTM* (Bottom Right)

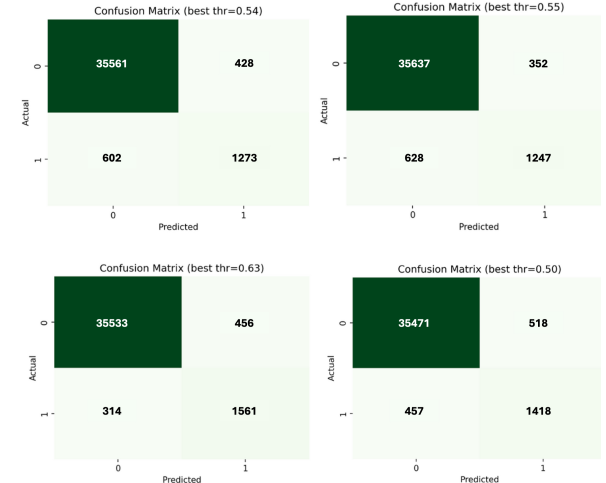


Figure 6: Confusion matrices of all 4 models at optimized thresholds. *TCN* (Top Left), *Medformer* (Top Right), *ST-Transformer* (Bottom Left), *BiLSTM* (Bottom Right)

precision-recall curves for each model at different

thresholds; ‘*’ indicates the best threshold in both Figures 5 and 4. We also present confusion matrices (Figure 6) at their optimized thresholds.

Identifying hypoxia in real-world operational settings is challenging. Thus, we are most interested in correct prediction of true negatives to avoid false alarms (predicting hypoxia when conditions are normoxic). ST-Transformer predicted the largest number of True Negatives (1561) at optimized threshold versus 1320 at the default threshold. This demonstrates that the ST-Transformer model, when combined with the spatial and temporal signals, better learns the pattern of hypoxia and avoids false alarms.

Brier Score. We also use calibration metrics to assess model prediction quality. *Brier Score* (BS) provides the mean-squared error of probabilistic predictions for binary outcomes. A lower Brier score indicates more accurate predictions ranging from 0.0 (perfect) to 1.0 (worst possible):

$$BS = \frac{1}{N} \sum_{i=1}^N (p_i - y_i)^2 \quad (10)$$

with N being the cardinality of the set of samples, $p_i \in [0, 1]$ being the predicted probability of the positive class, and $y_i \in \{0, 1\}$ being the ground truth outcome.

We observe the BS value of each model across our 4 test datasets in Table 2. For August 2020 test data, all models showed low BS indicating good performance. As an example of high variability due to real-world test data, consider Medformer. With August 2020 data we have BS 0.0291 compared to the real-world data (Summers 2022-24) in which Medformer achieved the highest BS of all models (0.2417). In contrast, BiLSTM and ST-Transformer were consistent across all test periods with BS varying by ± 0.037 and ± 0.040 , respectively. This demonstrates the reliability of BiLSTM and ST-Transformer for operational deployment.

Log loss. Log loss (cross-entropy) is a calibration metric that evaluates probabilistic prediction accuracy by penalizing confident wrong predictions more heavily:

Table 2: Log Loss and Brier Score for 4 timeframes across each model’s prediction.

Dataset	Model	Brier Score	Log Loss
August 2020	BiLSTM	0.0215	0.0846
	Medformer	0.0291	0.1252
	ST-Transformer	0.0282	0.1422
	TCN	0.0237	0.0904
Summer 2022	BiLSTM	0.0589	0.2117
	Medformer	0.2043	0.5902
	ST-Transformer	0.0686	0.2663
	TCN	0.1386	0.4443
Summer 2023	BiLSTM	0.0532	0.1953
	Medformer	0.2417	0.6733
	ST-Transformer	0.0580	0.2367
	TCN	0.2612	0.7812
Summer 2024	BiLSTM	0.0416	0.1591
	Medformer	0.0915	0.3069
	ST-Transformer	0.0530	0.2219
	TCN	0.0575	0.2147

$$\text{LogLoss} = -\frac{1}{N} \sum_{i=1}^N [z_i \log(q_i) + (1 - z_i) \log(1 - q_i)] \quad (11)$$

where N is the number of samples, where q_i is the probability predicted for the i th sample, and z_i is the observed binary label.

Like BS, log loss ranges from 0.0 (perfect predictions) to infinity (confident but incorrect predictions). For a balanced binary result, random guessing with $p = 0.5$ yields a log loss of approximately 0.693.

In Table 2, a log loss value greater than 0.693 was only achieved by TCN (0.7812) with Summer 2023 data, although Medformer was close (0.6733). This indicates that TCN performed worse than random guessing on Summer 2023 data. In contrast, low log loss across all tests for BiLSTM and ST-Transformer indicates strong performance with real-time data.

6.2 Pairwise Model Comparison with McNemar’s Test

We apply McNemar’s test to determine whether the performance differences between models are statistically significant. McNemar’s test is appropriate for

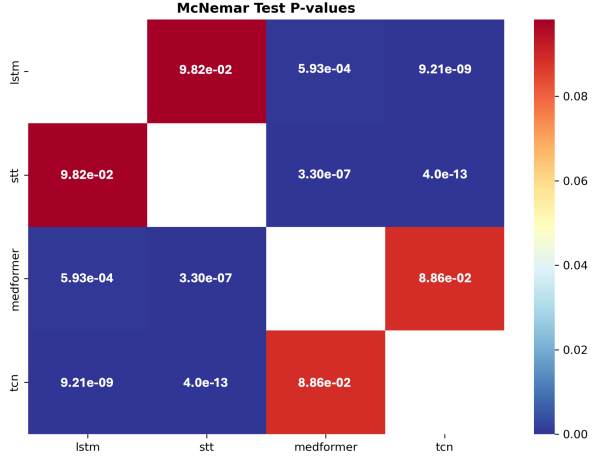


Figure 7: Pairwise McNemar test p -values across all models using August 2020 test data.

binary classification comparisons. The implementation constructs contingency tables capturing patterns of agreement and disagreement between model predictions. The test statistic is calculated as:

$$\chi^2 = \frac{(b - c)^2}{b + c} \quad (12)$$

with b and c respectively being the number of discordant pairs having outcomes $(1, 0)$ and $(0, 1)$. p -values are computed by using the cumulative distribution function of the χ^2 distribution for each pair of models.

Figure 7 shows the p -values for all pairwise comparisons using August 2020 test data. Four out of six model pairs demonstrated particularly strong significance ($p < 0.001$) observed for several comparisons including ST-Transformer vs TCN ($p = 4.0e-13$), ST-Transformer vs Medformer ($p = 3.30e-07$), BiLSTM vs TCN ($p = 9.21e-09$), and BiLSTM vs Medformer ($p = 5.93e-04$). However, differences between BiLSTM and ST-Transformer ($p = 0.0982$) and between Medformer and TCN ($p = 0.0886$) did not reach the conventional 0.05 significance threshold, indicating these model pairs have statistically similar predictions.

Effect size analysis. While McNemar's test revealed statistically significant differences between

Table 3: Pairwise effect sizes (Cohen's w) between models ($p < 0.001$).

Dataset	Model	BiLSTM	Medformer	ST-Transformer	TCN
Summer 2022	BiLSTM	-	0.9962	1.5288	1.2687
	Medformer	0.9962	-	1.0243	0.9046
	ST-Transformer	1.5288	1.0243	-	1.2890
	TCN	1.2687	0.9046	1.2890	-
Summer 2023	BiLSTM	-	0.9101	1.5655	0.9582
	Medformer	0.9101	-	0.9448	0.6467
	ST-Transformer	1.5655	0.9448	-	0.9875
	TCN	0.9582	0.6467	0.9875	-
Summer 2024	BiLSTM	-	1.4204	1.5922	1.5547
	Medformer	1.4204	-	1.4333	1.4236
	ST-Transformer	1.5922	1.4333	-	1.5626
	TCN	1.5547	1.4236	1.5626	-

model pairs, effect size measures the magnitude of those differences. Effect size helps identify which model strikes the most favorable balance between accuracy and computational overhead, even in cases where statistical significance was not achieved.

In Table 3 we report effect sizes between models derived from McNemar's test with $p < 0.001$. We use Cohen's w as the measure of effect size:

$$w = \sqrt{\frac{\chi^2}{N}} \quad (13)$$

where χ^2 is the chi-square statistic from McNemar's test and N is the total sample size. We observe that all pairwise comparison values exceeded Cohen's threshold for large effects (commonly ≥ 0.5). This indicates that the performance difference between models cannot be attributed to minor variations.

In terms of model-specific patterns, the BiLSTM and ST-Transformer comparison resulted in the highest Cohen's w values in each year (1.5288, 1.5655, and 1.5922, respectively for Summer 2022 through 2024). The high values indicate that BiLSTM and ST-Transformer fundamentally capture different aspects of the underlying temporal patterns. In comparison, the Medformer and TCN Cohen's w values showed the smallest effect sizes, but they are still substantial ranging from 0.6467 to 1.4236.

6.3 Spatial Validation

Spatial validation determines whether a model can capture the underlying oceanographic processes.

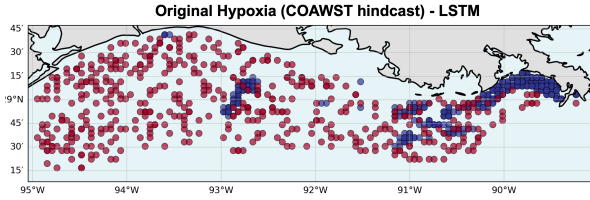


Figure 8: ROMS plot of August 2020 test data: COAWST hindcast showing hypoxia (blue dots) and normoxia (red dots).

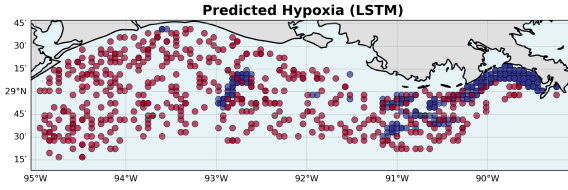


Figure 9: ROMS plot of August 2020 test data predicted using BiLSTM.

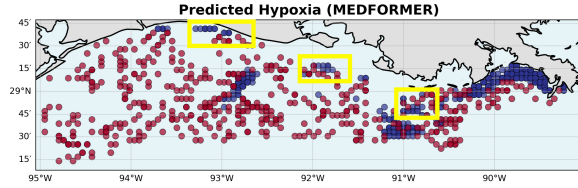


Figure 10: ROMS plot of August 2020 test data predicted using MedFormer.

We validated model predictions by plotting them against ROMS hindcast spatial data. Figure 8 shows a random sample of COAWST hindcast hypoxia (blue) and normoxia (red) for August 2020 test data. We see a group of blue dots indicating hypoxic conditions (oxygen $< 2.0\text{mg/L}$) concentrated near the Gulf shores. This coastal pattern reflects nutrient loading and Mississippi River freshwater outflow.

Figures 9 and 10 show BiLSTM and Medformer predictions, respectively, for the same test data. BiLSTM predictions align well with the events observed in Figure 8. However, Medformer shows clear misclassifications highlighted with yellow boxes in Figure

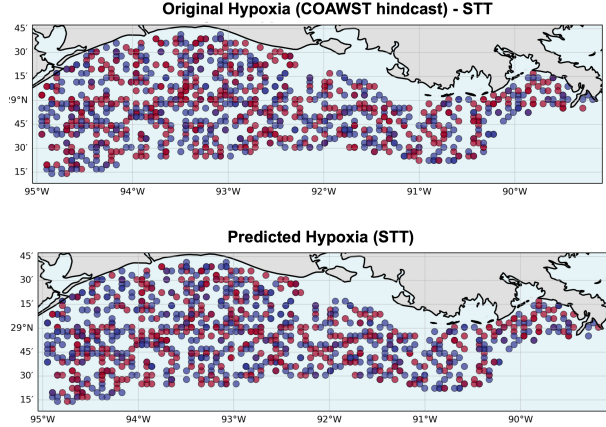


Figure 11: ROMS hindcast validation: COAWST hindcast versus ST-Transformer (best model) predictions for Summer 2022 (1000 random points).

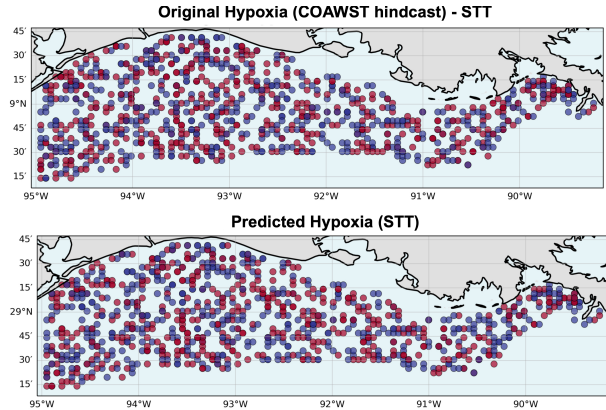


Figure 12: ROMS hindcast validation: COAWST hindcast versus ST-Transformer (best model) predictions for Summer 2023 (1000 random points).

10. Consistent with Table 1, BiLSTM is spatially superior to Medformer with the test data.

ST-Transformer demonstrates consistent spatial accuracy across our 2022-2024 test data; see Figures 11-13. ST-Transformer accurately captures coastal hypoxia patterns attributed to river-plume dynamics and stratification. These results support operational deployment of ST-Transformer and BiLSTM for fish-

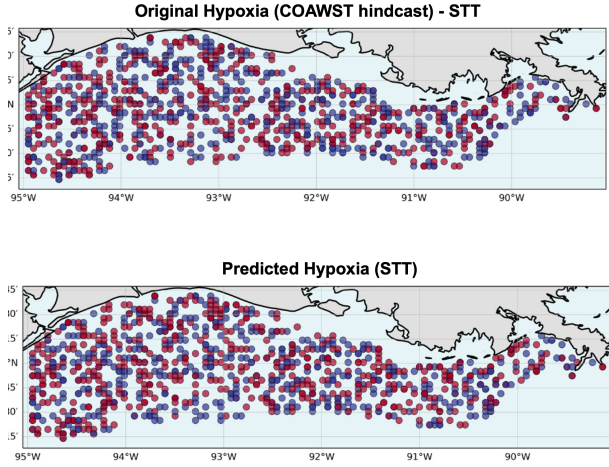


Figure 13: ROMS hindcast validation: COAWST hindcast versus ST-Transformer (best model) predictions for Summer 2024 (1000 random points).

ery management and field research planning.

7 Related Works

Different types of AI models have been used for diverse applications ranging from geospatial to robotics Sharma et al. [2018], Basu et al. [2015], Ou et al. [2025]. Below, we survey different AI-based approaches for coastal hypoxia and related applications. **Hypoxia prediction approaches.** Hypoxia prediction has evolved from seasonal statistical models to daily-resolution systems for the Gulf of Mexico. Katin et al. Katin et al. [2022] introduced daily Bayesian mechanistic forecasting explaining about 50% of the variability in hypoxic area. Ou et al. Ou et al. [2022] developed ensemble regression ($R^2 = 0.92$) combining generalized linear models (GLMs) and generalized additive models (GAMs). Using satellite-derived variables with a Random Forest model, Li et al. Li et al. [2023] predicted bottom dissolved oxygen with $\pm 1.2 - 1.4$ mg/L accuracy.

Ou et al. Ou et al. [2025] proposed a multi-classifier model combining U-net and DeepLabv3+ for Louisiana-Texas shelf spatial hypoxia prediction. Their approach achieved remarkable computa-

tional speedup from 1800s to 1s all while maintaining ROMS-compatible accuracy using the same environmental variables (PEA, sediment oxygen consumption, and temperature-dependent decomposition). However, their spatial segmentation approach treats daily forecasts independently, thus missing the temporal dependencies that result in hypoxia development over multiple days. This work is most similar to ours, but our sequence-based approach was developed to capture these temporal patterns driving hypoxic events.

Time series deep learning. In the literature, architecture comparison studies reveal performance dependencies on temporal characteristics. Pölz et al. Pölz et al. [2024] demonstrated that a Transformer outperformed a LSTM by about 9% for longer-timescale hydrological systems but underperformed by roughly 4% for shorter timescales. At six locations near China, Fu et al. Fu et al. [2024] demonstrated that a hybrid LSTM-Transformer achieved superior performance compared to individual architectures for prediction of sea surface temperature. Yan et al. Yan et al. [2020] reported that TCNs achieved competitive skill for El Niño-Southern Oscillation (ENSO) forecasting across multiple lead times (1 month, 3 months, 6 months, and 12 months Yan et al. [2020]), demonstrating the ability of TCNs to effectively capture long-range dependencies for climate prediction tasks. Wu et al. Wu et al. [2024] introduced physics-informed Transformers for ocean temperature and salinity prediction, while Zhang et al. Zhang and Awang [2025] developed spatio-temporal attention mechanisms applied to ambient air pollution forecasting. Together, these and other works demonstrate that Transformer-based architectures are well-suited for environmental applications.

Research gaps and our contributions. A comparison of temporal deep learning architectures for Gulf hypoxia prediction under identical conditions is lacking. We also observe other gaps in the literature. Medformer and spatio-temporal attention models (i.e., Transformer model variants) remain un-evaluated for coastal hypoxia prediction. In addition, environmental AI studies do not often compare performance of architectures using formal statistical significance tests. To address both of these issues, we

applied McNemar’s test (Section 6) on paired classification outcomes to evaluate the differences observed across four different architectures, including two Transformer architectures.

8 Conclusions

We compared four deep learning architectures for daily coastal hypoxia forecasting using consistent data preparation, experimental conditions, and evaluation protocols. We found ST-Transformer achieved the highest AUC-ROC values (0.982-0.992) and the highest metrics across all test periods (2020, 2022-2024). While McNemar’s test indicated that differences between ST-Transformer and BiLSTM did not reach statistical significance ($p = 0.098$), ST-Transformer’s higher performance metrics for all test years suggest practical advantages for operational deployment. This demonstrates the value of spatio-temporal modeling capabilities for predicting hypoxia in the Gulf of Mexico.. Future work will examine the transferability Collier et al. [2018] of these models to other costal locations where hypoxic conditions can occur.

References

Saikat Basu, Sangram Ganguly, Supratik Mukhopadhyay, Robert DiBiano, Manohar Karki, and Ramakrishna Nemani. Deepsat: a learning framework for satellite imagery. In *Proceedings of the 23rd SIGSPATIAL international conference on advances in geographic information systems*, pages 1–10, 2015.

Nitesh V. Chawla, Kevin W. Bowyer, Lawrence O. Hall, and W. Philip Kegelmeyer. Smote: synthetic minority over-sampling technique. *J. Artif. Int. Res.*, 16(1):321–357, June 2002. ISSN 1076-9757.

Edward Collier, Robert DiBiano, and Supratik Mukhopadhyay. Cactusnets: Layer applicability as a metric for transfer learning. In *2018 International Joint Conference on Neural Networks (IJCNN)*, pages 1–8. IEEE, 2018.

Katja Fennel et al. Sensitivity of hypoxia predictions for the northern gulf of mexico to sediment oxygen consumption and model nesting. *Journal of Geophysical Research: Oceans*, 118(2):990–1002, 2013. URL <https://doi.org/10.1002/jgrc.20077>.

Yu Fu, Jun Song, Junru Guo, Yanzhao Fu, and Yu Cai. Prediction and analysis of sea surface temperature based on lstm-transformer model. *Regional Studies in Marine Science*, 78:103726, 2024. ISSN 2352-4855. URL <https://doi.org/10.1016/j.rsma.2024.103726>.

Alex Graves and Jürgen Schmidhuber. Frame-wise phoneme classification with bidirectional lstm and other neural network architectures. *Neural Networks*, 18(5):602–610, 2005. ISSN 0893-6080. URL <https://doi.org/10.1016/j.neunet.2005.06.042>. IJCNN 2005.

A. Katin, D. Del Giudice, and D. R. Obenour. Temporally resolved coastal hypoxia forecasting and uncertainty assessment via bayesian mechanistic modeling. *Hydrology and Earth System Sciences*, 26(4):1131–1143, 2022. doi: 10.5194/hess-26-1131-2022. URL <https://hess.copernicus.org/articles/26/1131/2022/>.

Michio J. Kishi et al. Nemuro—a lower trophic level model for the north pacific marine ecosystem. *Ecological Modelling*, 202(1):12–25, 2007. ISSN 0304-3800. doi: 10.1016/j.ecolmodel.2006.08.021. URL <https://doi.org/10.1016/j.ecolmodel.2006.08.021>. Special Issue on NE-MURO (North Pacific Ecosystem Model for Understanding Regional Oceanography) and NE-MURO.FISH (NEMURO for Including Saury and Herring).

T. Kätterer, M. Reichstein, O. Andrén, and A. Lomander. Temperature dependence of organic matter decomposition: a critical review using literature data analyzed with different models. *Biology and Fertility of Soils*, 27(3):258–262, 1998. ISSN 1432-0789. doi: 10.1007/s003740050430. URL <https://doi.org/10.1007/s003740050430>.

Colin Lea, Rene Vidal, Austin Reiter, and Gregory D. Hager. Temporal convolutional networks: A unified approach to action segmentation, 2016. URL <https://arxiv.org/abs/1608.08242>.

Yingjie Li, Samuel V.J. Robinson, Lan H. Nguyen, and Jianguo Liu. Satellite prediction of coastal hypoxia in the northern gulf of mexico. *Remote Sensing of Environment*, 284:113346, 2023. ISSN 0034-4257. doi: <https://doi.org/10.1016/j.rse.2022.113346>. URL <https://doi.org/10.1016/j.rse.2022.113346>.

V. R. R. Matli and D. Obenour. Trends and drivers of hypoxic thickness and volume in the northern gulf of mexico: 1985–2018. *PLOS ONE*, 19(12):e0302759, 2024. doi: 10.1371/journal.pone.0302759. URL <https://doi.org/10.1371/journal.pone.0302759>.

NOAA. Gulf of mexico ‘dead zone’ larger than average, scientists find. <https://www.noaa.gov/news-release/gulf-of-mexico-dead-zone-larger-than-average-scientists-find>. August 2024. Accessed: 2025-08-08.

Y. Ou. Dataset for ”forecasting coastal hypoxia using a blend of numeric and artificial intelligence models”. <http://www.hydroshare.org/resource/0cc2093cc67543fd82b06d6b5b9c79e4>, 2024. HydroShare.

Y. Ou, B. Li, and Z. G. Xue. Hydrodynamic and biochemical impacts on the development of hypoxia in the louisiana–texas shelf – part 2: statistical modeling and hypoxia prediction. *Biogeosciences*, 19(15):3575–3593, 2022. doi: 10.5194/bg-19-3575-2022. URL <https://bg.copernicus.org/articles/19/3575/2022/>.

Yanda Ou, Z. George Xue, Supratik Mukhopadhyay, Magesh Rajasekaran, and Dylan Wichman. Forecasting coastal hypoxia using a blend of mechanistic and artificial intelligence models. *Scientific Reports*, 15(1):31452, 2025. ISSN 2045-2322. doi: 10.1038/s41598-025-17053-7. URL <https://doi.org/10.1038/s41598-025-17053-7>.

Anna Pölz et al. Transformer versus lstm: A comparison of deep learning models for karst spring discharge forecasting. *Water Resources Research*, 60(4):e2022WR032602, 2024. URL <https://doi.org/10.1029/2022WR032602>.

M. Schuster and K.K. Paliwal. Bidirectional recurrent neural networks. *IEEE Transactions on Signal Processing*, 45(11):2673–2681, 1997. URL <https://doi.org/10.1109/78.650093>.

Gokarna Sharma, Rusul Alsaedi, Costas Busch, and Supratik Mukhopadhyay. The complete visibility problem for fat robots with lights. In *Proceedings of the 19th International Conference on Distributed Computing and Networking*, pages 1–4, 2018.

Alexander F. Shchepetkin and James C. McWilliams. The regional oceanic modeling system (roms): a split-explicit, free-surface, topography-following-coordinate oceanic model. *Ocean Modelling*, 9(4):347–404, 2005. ISSN 1463-5003. doi: 10.1016/j.ocemod.2004.08.002. URL <https://doi.org/10.1016/j.ocemod.2004.08.002>.

Yihe Wang, Nan Huang, Taida Li, Yujun Yan, and Xiang Zhang. Medformer: A multi-granularity patching transformer for medical time-series classification. 2024. URL <https://arxiv.org/abs/2405.19363>.

John C. Warner, Brandy Armstrong, Ruoying He, and Joseph B. Zambon. Development of a coupled ocean–atmosphere–wave–sediment transport (coawst) modeling system. *Ocean Modelling*, 35 (3):230–244, 2010. ISSN 1463-5003. doi: 10.1016/j.ocemod.2010.07.010. URL <https://doi.org/10.1016/j.ocemod.2010.07.010>.

Song Wu et al. Pgtransnet: a physics-guided transformer network for 3d ocean temperature and salinity predicting in tropical pacific. *Frontiers in Marine Science*, Volume 11 - 2024, 2024. ISSN 2296-7745. doi: 10.3389/fmars.2024.1477710. URL <https://doi.org/10.3389/fmars.2024.1477710>.

Jining Yan, Lin Mu, Lizhe Wang, Rajiv Ranjan, and Albert Y. Zomaya. Temporal convolutional networks for the advance prediction of enso. *Scientific Reports*, 10(1):8055, 2020. ISSN 2045-2322. doi: 10.1038/s41598-020-65070-5. URL <https://doi.org/10.1038/s41598-020-65070-5>.

Yujie You, Le Zhang, Peng Tao, Suran Liu, and Luonan Chen. Spatiotemporal transformer neural network for time-series forecasting. *Entropy*, 24(11), 2022. ISSN 1099-4300. doi: 10.3390/e24111651. URL <https://doi.org/10.3390/e24111651>.

Liuqian Yu, Katja Fennel, and Arnaud Laurent. A modeling study of physical controls on hypoxia generation in the northern gulf of mexico. *Journal of Geophysical Research: Oceans*, 120(7):5019–5039, 2015. doi: 10.1002/2014JC010634. URL <https://doi.org/10.1002/2014JC010634>.

Rui Zhang and Norhashidah Awang. A novel stitransformer model for spatio-temporal ambient air pollution forecasting. *Journal of Big Data*, 12(1):101, 2025. ISSN 2196-1115. doi: 10.1186/s40537-025-01150-5. URL <https://doi.org/10.1186/s40537-025-01150-5>.